ORIGINAL PAPER

Ab initio studies on the reactivity of the CF_3OCH_2O radical: Thermal decomposition vs. reaction with O_2

Hari Ji Singh · Bhupesh Kumar Mishra

Abstract Hydrofluoroethers are being considered as potential candidates for third generation refrigerants. The present investigation involves the *ab initio* quantum mechanical study of the decomposition mechanism of CF_3OCH_2O radical formed from a hydrofluoroether, CF_3OCH_3 (HFE-143a) in the atmosphere. The geometries of the reactant, products and transition states involved in the decomposition pathways are optimized and characterized at the DFT (B3LYP) level of theory using 6-311G(d,p) basis set. Energy calculations have been performed at the G2(MP2) and G2M (CC,MP2) level of theory. Two prominent decomposition channels, C-O bond scission and reaction with atmospheric O_2 have been considered for detailed investigation. Studies performed at the G2(MP2) level reveals that the decomposition channel involving C-O bond scission occurs with a barrier height of 23.8 kcal mol^{-1} whereas the oxidative pathway occurring with O_2 proceeds with an energy barrier of 7.2 kcal mol^{-1}. On the other hand the corresponding values at G2M(CC,MP2) are 24.5 and 5.9 kcal mol^{-1} respectively. Using canonical transition state theory (CTST) rate constants for the two pathways considered are calculated at 298 K and 1 atm pressure and found to be 5.9×10^{-6} s^{-1} and 2.3×10^{-5} s^{-1} respectively. The present study concludes that reaction with O_2 is the dominant path for the consumption of CF_3OCH_2O in the atmosphere. Transition states are searched and characterized on the potential energy surfaces involved in both of the reaction channels. The existence of transition state on the corresponding potential energy surface is ascertained by performing intrinsic reaction coordinate (IRC) calculation.

Introduction

It is now a well accepted fact that the release of manmade chlorofluorocarbons (CFCs) is responsible for the depletion of ozone layer in the stratospheric region of the atmosphere [1–4]. CFCs are chemically inert species and inspite of this being a desired property for their industrial applications it is this that causes them to have a deleterious effect on the environment. Once released into the atmosphere CFCs remain there for a longer period of time because of their chemical inertness. Consequently, they reach the stratospheric region of the Earth's atmosphere without being removed through any action. Once in the stratosphere they are broken down by UV radiations releasing chlorine atoms that initiate chain processes destroying ozone.

On account of the ozone depletion caused by CFCs, global alarm was raised and serious attempts had been made in the past decade or so to find out its alternatives. Hydrochlorofluorocarbons (HCFCs) and hydrofluorocarbons (HFCs) have been synthesized and used as alternatives of CFCs as second generation refrigerants [5, 6]. However, studies performed with many of the HFCs and HCFCs have shown that these are not a viable solution to protect the

H. J. Singh (✉) · B. K. Mishra
Department of Chemistry, DDU Gorakhpur University,
Gorakhpur 273009, India
e-mail: hari_singh81@hotmail.com

ozone layer because of their significant global warming potentialities [7, 8]. Recently, hydrofluoroethers (HFEs) have drawn considerable attention as third generation replacement of CFCs that may be used as cleaning agents of electronic equipments, heat transfer agents in refrigeration systems and carrier fluids for lubricant deposition [9–11]. It is presumed that the absence of chlorine atoms in HFEs would have little impact on stratospheric ozone as they would be likely to possess a negligible ozone depleting potential (ODP) because of their short life times [12, 13]. Such a presumption has indeed been substantiated by *ab initio* and semi-empirical calculations performed by Cooper *et al.* [14, 15]. However, the presence of C-F and C-O bonds in HFEs may enhance their absorption features in the atmospheric infrared region (800–1400 cm^{-1}) and could play a significant role as green house gases [16]. Therefore, considerable attention has been paid in recent years to perform experimental and theoretical studies on the decomposition of HFEs in order to find its suitability as a replacement of HCFCs and HFCs [16–19].

One of the important hydrofluoroethers, HFE-143a belongs to a class of compounds which has been developed to replace commonly used refrigerant HFC-143a. Once released into the atmosphere HFE-143a undergoes degradation by reaction with photochemically produced hydroxyl radicals [20]. A general mechanism of tropospheric degradation of HFE-143a may be shown as follows:

As shown in Scheme 1 the degradation of HFE-143a is initiated by the attack of OH radicals yielding halogenated alkyl radicals (CF$_3$OCH$_2$•) which rapidly react with atmospheric O$_2$ to form peroxy radicals (CF$_3$OCH$_2$O$_2$•). The latter can react with NO$_x$ (x=1, 2) and HO$_2$ present in the troposphere ultimately leading to the formation of
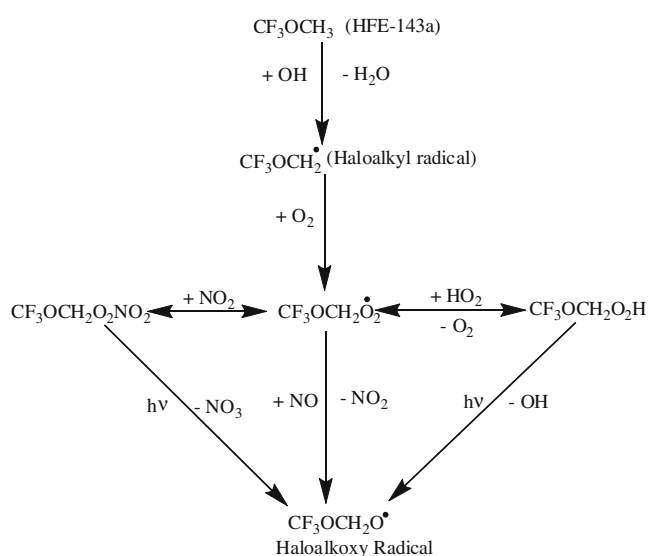
haloalkoxy radicals (CF$_3$OCH$_2$O•). The haloalkoxy radicals thus formed play an important role in the depletion of most of the organic compounds present in the atmosphere [21]. The depletion of alkoxy radical may occur *via* two different pathways. It may undergo unimolecular decomposition or react with O$_2$ [22] involving C - O and C - H bond scission as shown below:

$$CF_3OCH_2O \rightarrow CF_3O + CH_2O \qquad (1)$$

$$CF_3OCH_2O + O_2 \rightarrow CF_3OC(O)H + HO_2 \qquad (2)$$
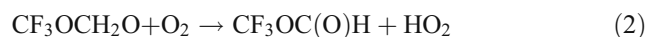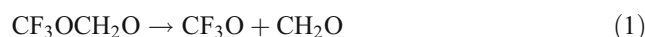
Due to the significant role played by haloalkoxy radicals formed from hydrofluoroethers in the destruction of a variety of organic compounds released into the atmosphere, studying the fate of CF$_3$OCH$_2$O formed from HFE-143a is needed from the viewpoint of understanding its role in atmospheric chemistry. There are only a few studies on the kinetics and decomposition mechanism of HFE-143a [23–25]. Using *ab initio* methods Good and Francisco [25] studied the structure and vibrational spectra of HFE-143a. Additionally, in an experimental study utilizing smog chamber/FTIR technique, Christensen *et al.* [23] concluded that the fate of haloalkoxy radical formed from HFE-143a was its reaction with O$_2$ and not its thermal decomposition. Thus, there is a desirable need to perform high level *ab initio* quantum mechanical calculations to determine the energetics involved during the decomposition of CF$_3$OCH$_2$O. In the present investigation we performed a computational study on the decomposition pathways of CF$_3$OCH$_2$O radical involving C-O and C-C bond scission as given by reactions (1) and (2) using high-level molecular orbital methods. Rate constants for the above two channels considered are calculated by utilizing canonical transition state theory (CTST). Attempts have been made to search for transition states on the corresponding potential energy surfaces and energy barriers are calculated. Existence of transition states is ascertained by making intrinsic reaction coordinate (IRC) calculation.

Computational methods

All calculations performed during the course of the present investigation are made using the GAUSSIAN 03 series of program [26]. Amongst a series of available theories of calculation the B3LYP/6-311G(d,p) [27, 28] method has been found to yield sufficiently accurate results in predicting reliable geometries of the species at stationary points. Additionally, it is found to be computationally inexpensive for scanning the potential energy surface. Therefore, geometries of reactants, products and transition states involved in reactions (1) and (2) have been optimized at

Scheme 1 Tropospheric degradation of HFE-143a

the DFT(B3LYP)/6-311G(d,p) level. Vibrational frequency calculations have been performed for the characterization of stationary points on the potential energy surface of the reactions involved. These have been identified to correspond to local minima with all positive values of vibrational frequencies (NIMAG=0). Zero point energy (ZPE) and rate constant calculations have also been performed at the same level of theory. Transition state is characterized by the occurrence of only one imaginary frequency (NIMAG=1) on the potential energy surface. To confirm that there is a smooth transition from reactants to products through the observed transition state, IRC calculations [29] are performed with the same level of theory at which the geometry optimization and frequency calculation have been performed.

Energetics of the reactions considered are studied using two variants of G2 methodology [30], the G2(MP2) [31], and G2M(CC,MP2) [32]. Mebel *et al.* [32] suggested that G2M(CC,MP2) method was most suited to systems containing more than six to seven heavy atoms. In both methods, the

geometry optimization and frequency calculation are performed at B3LYP/6-311G(d,p) level and zero point energy (ZPE) values are determined. In the G2(MP2) method, MP2 calculations are performed instead of MP4 for the basis set extension corrections which is considered to reasonably approximate the full G2 method at a substantially reduced computational cost and is more suitable for considerably large systems. The G2(MP2) energy is calculated as:

$$E[G2(MP2)] = E_{base} + \Delta E(MP2) + HLC + ZPE$$

where,

$$E_{base} = E[QCISD(T)/6-311G(d,p)],$$
$$\Delta E(MP2) = E[MP2/6-311+G(3df,2p)]$$
$$- E[MP2/6-311G(d,p)],$$

and HLC and ZPE are the high level correction and zero point energy. HLC is determined as:

$$HLC = -0.00525n_\alpha - 0.00019n_\beta$$

Fig. 1 Optimized geometries of reactants, products, and transition states involved in the decomposition pathways of CF$_3$OCH$_2$O radical obtained at B3LYP/6-311G (d,p) level
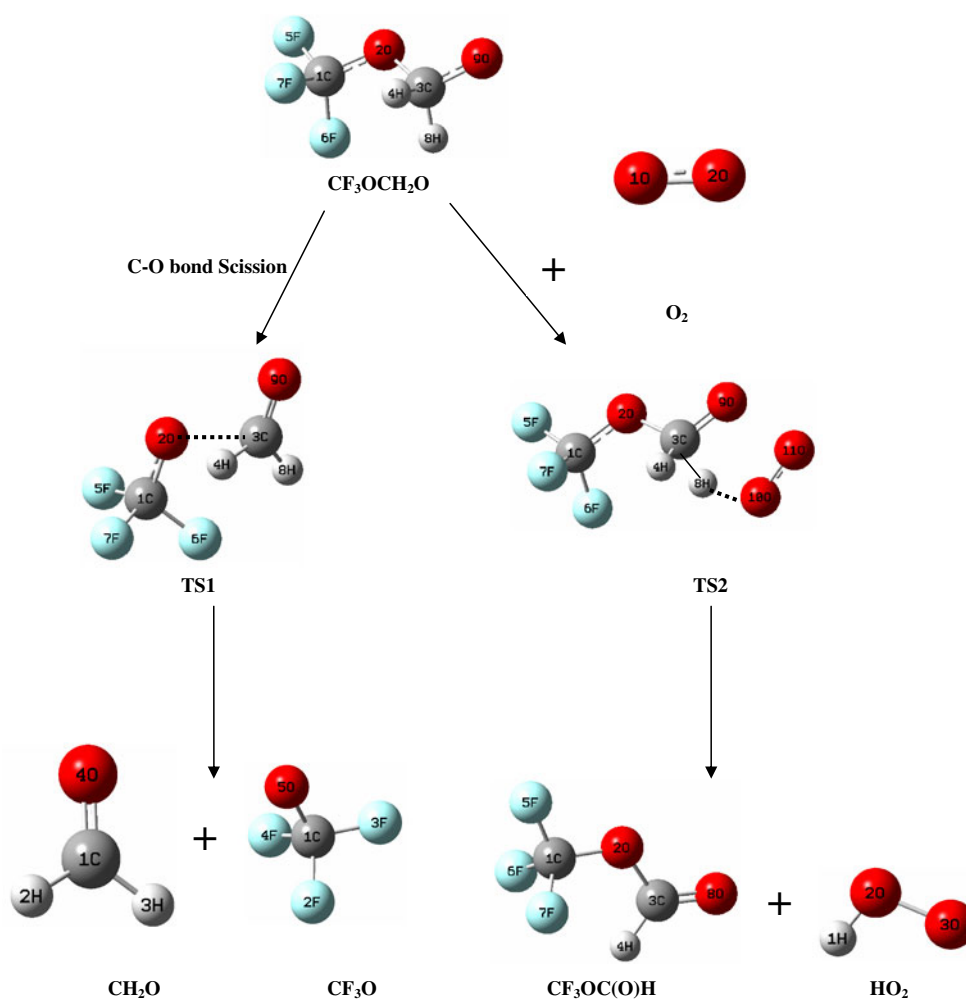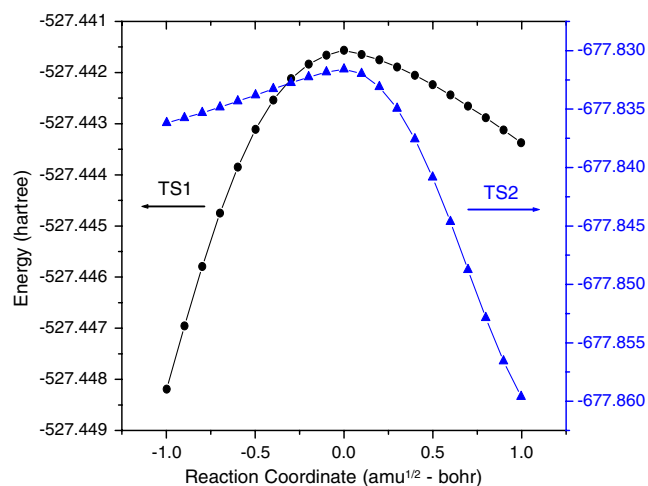
Table 1 Structural parameters of reactant, products, and transition states involved in CF_3O-CH_2O decomposition at B3LYP/ 6–311G(d,p) level of theory

	CF_3OCH_2O	TS1	TS2	CF_3O	CH_2O	$CF_3OC(O)H$
Bond length (Å)						
R (C1-F5)	1.328	1.343	1.327	——	——	1.323
R (C1-F6)	1.356	1.373	1.356	——	——	1.344
R (C1-F7)	1.356	1.356	1.354	——	——	1.344
R (C1-F2)	——	——	——	1.336	——	——
R (C1-F4)	——	——	——	1.340	——	——
R (C1-O2)	1.339	1.319	1.343	——	——	1.366
R (C3-O2)	1.458	1.984	1.458	——	——	1.394
R (C3-O9)	1.309	1.202	1.252	——	——	——
R (C1-O5)	——	——	——	1.350	——	——
R (C1-O4)	——	——	——	——	1.200	——
R (C3-H4)	1.108	1.127	1.104	1.081	——	1.097
R (C3-H8)	1.108	1.098	1.229	——	——	1.181
R (C1-H2)	——	——	——	——	1.109	——
R (C1-H3)	——	——	——	——	1.109	——
R (O10-O11)	——	——	1.211	——	——	——
R (H8-O10)	——	——	1.490	——	——	——
Bond Angle (deg)						
A (O2-C1-F5)	109.162	110.524	109.076	——	——	108.168
A (O2-C1-F6)	112.381	112.851	112.177	——	——	111.606
A (O2-C1-F7)	121.386	112.963	112.477	——	——	111.606
A (F5-C1-F6)	108.357	106.965	108.400	——	——	109.068
A (F5-C1-F7)	108.354	107.797	108.415	——	——	109.068
A (F6-C1-F7)	106.032	105.370	106.169	——	——	107.275
A (F2-C1-F3)	——	——	——	107.538	——	——
A (F2-C1-F4)	——	——	——	109.521	——	——
A (C1-O2-C3)	116.105	116.511	116.610	——	——	117.664
A (O2-C3-H4)	108.618	68.265	110.431	——	——	113.056
A (O2-C3-H8)	108.609	98.220	104.502	——	——	120.387
A (O2-C3-O9)	112.155	113.204	115.074	——	——	——
A (H4-C3-H8)	107.315	114.981	101.747	——	——	126.556
A (H2-C1-H3)	——	——	——	——	115.503	——
A (H4-C3-O9)	109.998	118.551	119.503	——	——	——
A (H8-C3-O9)	110.005	124.677	109.103	——	——	——
A (H2-C1-O4)	——	——	——	——	122.248	——

Table 2 Unscaled vibrational frequencies of reactant, products, and transition states involved in CF_3OCH_2O decomposition calculated at B3LYP/ 6–311G(d,p) level of theory

Species	Vibrational frequencies (cm^{-1})
CF_3OCH_2O	45, 102, 191, 396, 429, 447, 600, 607, 685, 788, 867, 994, 1130, 1167, 1174, 1216, 1282, 1341, 1395, 2886, 2909
TS1	***408i***, 33, 90, 145, 343, 400, 420, 546, 604, 629, 656, 866, 972, 1059, 1117, 1158, 1246, 1349, 1662, 2689, 3019
TS2	***1081i***, 27, 56, 121, 158, 170, 228, 389, 433, 461, 532, 604, 610, 666, 691, 868, 973, 1082, 1141, 1216, 1230, 1276, 1309, 1409, 1544, 1702, 2946
$CF_3OC(O)$ H	81, 108, 199, 414, 430, 477, 611, 612, 720, 912, 1018, 1051, 1186, 1221, 1285, 1425, 1893, 3050
CF_3O	266, 403, 571, 590, 612, 889, 1152, 1202, 1260
CH_2O	1201, 1270, 1538, 1826, 2870, 2919
HO_2	1162, 1427, 3612
O_2	1627

Fig. 2 IRC plots performed for transition states TS1 and TS2 obtained during thermal and oxidative decomposition of CF_3OCH_2O

where n_α and n_β are the number of α and β valence electrons with $n_\alpha \geq n_\beta$. On the other hand the G2M(CC, MP2) energy is calculated in the following manner:

$$E[G2M(CC, MP2)] = E_{base} + \Delta E(3df, 2p) + \Delta E(CC)$$
$$+ HLC + ZPE$$

where,

$$E_{base} = E[MP4/6 - 311G(d, p)],$$

$$\Delta E(3df, 2p) = E[MP2/6 - 311 + G(3df, 2p)]$$
$$- E[MP2/6 - 311G(d, p)],$$

and

$$\Delta E(CC) = E[CCSD(T)/6 - 311G(d, p)]$$
$$- E[MP4/6 - 311G(d, p)].$$

HLC and ZPE have the same meaning as described earlier. In this method single point energy calculation is performed

at MP2 and MP4 levels. For basis set correction CCSD(T)/ 6-311G(d,p) is substituted for the QCISD(T)/6-311G(d,p) of the original G2 method.

Results and discussion

The haloalkoxy radical (CF_3OCH_2O) studied during the course of the present investigation have H-atoms that are prone to be attacked by O_2. Thus, the two most plausible fates of this radical in the atmosphere are its thermal decomposition and reaction with O_2 as considered above by reactions (1) and (2). Optimized geometries of reactants, products, and transition states made at B3LYP /6-311G(d,p) level of theory are shown in Fig. 1 and their geometrical parameters are recorded in Table 1. Transition states are searched on the potential energy surface of reactions (1) and (2) and characterized as TS1 and TS2 respectively. Their optimized geometries are also shown in Fig. 1 and structural parameters are recorded in Table 1. Data recorded in Table 1 followed by visualization of the optimized structures using GaussView [33] reveals that in TS1 the elongation of the C - O bond occurs from 1.458 to 1.984 Å resulting is an increase in the bond length of about 36%. Similarly the results obtained for the optimized structure of TS2 reveal that C - H bond increases from 1.108 Å to 1.229 Å (approx. 11%). Results obtained during frequency calculations performed at B3LYP /6-311G(d,p) level for species of reactions (1) and (2) and the corresponding transition states are recorded in Table 2. These results show that the reactants and products have stable minima on their potential energy surface characterized by the occurrence of only real positive vibrational frequencies. Transition states TS1 and TS2 are characterized by the occurrence of only one imaginary frequency obtained at 408 and 1081 cm^{-1} respectively as recorded in Table 2. Visualization of the vibration corresponding to the calculated imaginary frequency using GaussView [33] shows a well defined transition state connecting reactants and products during transition. The existence of transition state on the potential energy surface is further ascertained by IRC calculation performed at the same

Table 3 Zero-point corrected total energy for species involved in C-O bond scission from CF_3OCH_2O decomposition. Geometries are optimized at B3LYP/6–311G(d, p) level. (unit: hartree)

Method	CF_3OCH_2O	TS1	CF_3O	CH_2O
B3LYP/6-311G(d,p)	−527.429076	−527.388439	−412.884580	−114.510909
MP2/6-311G(d, p)	−526.235398	−526.175394	−411.996155	−114.209562
MP2/6-311+G(3df,2p)	−526.553074	−526.496708	−412.237113	−114.280760
MP4/6-311G(d, p)	−526.301563	−526.244683	−412.036803	−114.236969
CCSD(T)/6-311G(d, p)	−526.297116	−526.250678	−412.032490	−114.234950
QCISD(T)/6-311G(d, p)	−526.299111	−526.253760	−412.033979	−114.235559
G2M(CC,MP2)	−526.720277	−526.681190	−412.366603	−114.323177
G2(MP2)	−526.722272	−526.684272	−412.368092	−114.323786

Table 4 Zero-point corrected total energy for species involved in reaction of CF_3OCH_2O with O_2. Geometries are optimized at B3LYP/6-311G (d, p) level. (unit: hartree)

| Method	$CF_3OCH_2O+O_2$	TS2	$CF_3OC(O)H$	HO_2
B3LYP/6-311G (d,p)	−677.728124	−677.714578	−526.905407	−150.936842
MP2/6-311G(d,p)	−676.255348	−676.222226	−525.738655	−150.571670
MP2/6-311+G(3df,2p)	−676.629388	−676.597243	−525.056705	−150.663022
MP4/6-311G(d,p)	−676.339855	−676.310502	−525.795688	−150.598723
CCSD(T)/6-311G(d,p)	−676.331863	−676.313795	−525.784603	−150.600947
QCISD (T)/6-311G(d,p)	−676.333858	−676.316903	−525.786926	−150.601748
G2M(CC,MP2)	−676.847642	−676.838156	−526.216921	−150.721879
G2(MP2)	−676.849630	−676.835048	−526.219244	−150.722680

level of theory. The minimum energy path is obtained by IRC calculation using Gonzalez - Schlegal steepest descent path [29] in the mass-weighted Cartesian coordinates with a step-size of 0.05 ($amu^{1/2}$- bohr) for each channel of decomposition. The IRC plots for TS1 and TS2 shown in Fig. 2 clearly show a smooth transition from reactants to products on the potential energy surface.

Single point energy calculations of various species involved in reactions (1) and (2) are performed using MP2, MP4, CCSD(T), and QCISD(T) level of theories at B3LYP/6-311G(d,p) optimized geometries. Zero point energy is also determined at B3LYP/6-311G(d,p) and corrected with a scale factor of 0.96 [34]. Zero-point corrected total energies using standard and extended basis sets for various species under consideration are recorded in Tables 3 and 4. Calculated energy values using G2(MP2) and G2M(CC,MP2) basis set additivity methods are also recorded in Tables 3 and 4. The associated energy barrier corresponding to reaction (1) and (2) determined from the data of Tables 3 and 4 and recorded in Table 5 show that the energy barrier for H-abstraction reaction of CF_3OCH_2O with molecular O_2 is in the range of 5–20 kcal mol^{-1} depending upon the level of theory used during the calculation whereas it is in the range of 23–37 kcal mol^{-1} for C-O bond scission occurred in its thermal decomposi-

tion. Results show that the G2(MP2) method yields a value of 23.8 and 7.2 kcal mol^{-1} for C-O bond scission and H-elimination by molecular O_2 respectively. On the other hand, the modified G2M(CC,MP2) method yields corresponding values as 24.5 and 5.9 kcal mol^{-1}. The corresponding energy barriers calculated at B3LYP is found to be 25.5 and 8.5 kcal mol^{-1} as recorded in Table 5. The calculated energy barriers for reactions (1) and (2) clearly show the dominance of H-elimination pathways involved during the oxidation of CF_3OCH_2O radical which is in accord with the conclusion made by Christensen *et al.* [23] in an experimental study involving smog chamber/FTIR technique. The energy barriers for reactions (1) and (2) calculated during the present investigation at G2(MP2) level are in good agreement with the values obtained by Good *et al.* [24] using DFT-B3LYP method with extended basis set as 21.2 and 7.6 kcal mol^{-1}. Using zero-point corrected total energy data as recorded in Tables 3 and 4, an energy level diagram for reactions (1) and (2) is constructed.

Table 5 Calculated energy barriers for the decomposition of CF_3OCH_2O radical in kcal mol^{-1}

Method	Reaction with O_2 (C-H bond scission)	Thermal decomposition (C-O bond scission)
B3LYP/6-311G (d,p)	8.5	25.5
MP2/6-311G (d,p)	20.7	37.6
MP2/6-311+G(3df,2p)	20.1	35.3
MP4/6-311G(d,p)	18.4	35.6
CCSD(T)/6-311G(d, p)	11.3	29.1
QCISD(T)/6-311G(d,p)	9.3	28.4
G2M(CC,MP2)	5.9	24.5
G2(MP2)	7.2	23.8
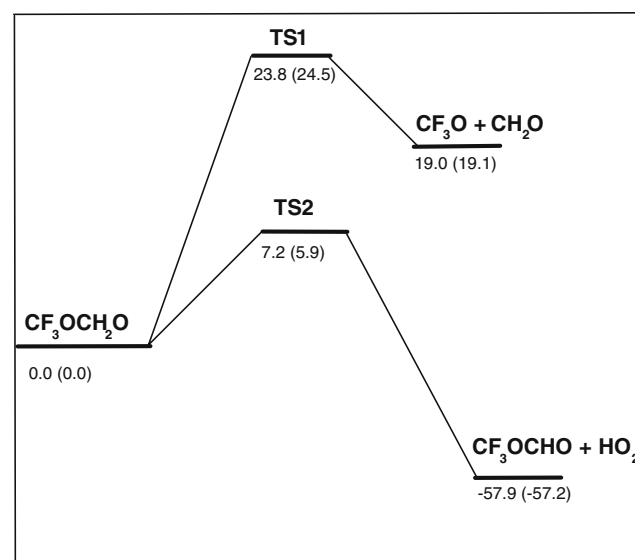
Fig. 3 Relative energy diagram in kcal mol^{-1} for the thermal and oxidative decomposition of CF_3OCH_2O at G2(MP2) and G2M(CC, MP2) levels. The values in parentheses are at G2M(CC,MP2)

These energies are plotted with respect to the ground state energy of CF_3OCH_2O arbitrarily taken as zero. Results are shown in Fig. 3. The values given in parentheses in Fig. 3 correspond to G2M(CC,MP2). It is evident from Fig. 3 that the oxidation pathway is dominant as compared to the thermal decomposition of CF_3OCH_2O. Calculations show that spin contamination is not important for the CF_3OCH_2O radical because $<S^2>$ is 0.76 at B3LYP/6–311G(d,p) before annihilation that are only slightly larger than the expected value of $<S^2> = 0.75$ for doublets.

Rate constants

The rate constants of reactions (1) and (2) responsible for the decay of CF_3OCH_2O radical are calculated using canonical transition state theory (CTST) [35] using the following expression:

$$k = \Gamma(T) \frac{k_B T}{h} \frac{Q^{\ddagger}_{TS}}{Q_R} \exp \frac{-\Delta E}{RT} \qquad (3)$$

where $\Gamma(T)$ is the tunneling correction factor at temperature T. $Q_{TS}^{\ddagger}$ and Q_R are the total partition functions for the transition state and reactant respectively. ΔE, k_B, and h have their usual meaning. The tunneling correction factor $\Gamma(T)$ is calculated by the expression given by Wigner [36] as

$$\Gamma(T) = 1 + \frac{1}{24} \left(\frac{h\nu^{\#}}{k_B T} \right)^2 \qquad (4)$$

where $\nu^{\#}$ is the imaginary frequency at the saddle point. The tunneling correction factor $\Gamma(T)$ is found to be almost unity. The partition functions for the respective transition state and reactant at 298 K are obtained from the harmonic vibrational frequencies calculations performed at the B3LYP/6–311G(d,p) level of theory that is being utilized for geometry optimization. The rate constant for C-O bond scission involving TS1 for CF_3OCH_2O decomposition is calculated to be 5.9×10^{-6} s^{-1} at 298 K and 1 atm pressure. Similar calculation performed for H-elimination occurring *via* reaction 2 involving TS2 as the transition state yields a rate constant of 2.3×10^{-5} s^{-1} at 298 K and 1 atm pressure. An extensive literature survey reveals that no experimental or theoretical data are available in the literature to make a comparison of the calculated values of rate constants obtained during the present investigation for CF_3OCH_2O radical decomposition. As a result we expect that the present study may provide useful information for future laboratory investigations.

Conclusions

The most important stationary points on the potential energy surface for the thermal decomposition of CF_3OCH_2O radical are determined using G2(MP2) and G2M(CC, MP2) methods on the geometries optimized at B3LYP/6–311G(d,p) for all the species involved during the decomposition channels of CF_3OCH_2O radical. Energetic calculation performed at G2 (MP2) and G2M(CC,MP2) levels reveals that the most dominant decomposition pathways for CF_3OCH_2O is its reaction with O_2. The thermal rate constants evaluated using canonical transition state theory (CTST) for the C- O bond scission and reaction with O_2 are calculated to be 5.9×10^{-6} s^{-1} and 2.3×10^{-5} s^{-1} respectively at 298 K and 1 atm pressure.

References

1. Solomon S (1990) Nature (London) 6291:347–354
2. Molina MJ, Rowland FS (1974) Nature 249:810–814
3. Rowland FS, Molina MJ (1994) Chem Eng News 8:72–76
4. Weubbles DJ (1983) J Geophys Res 88:1433–1443
5. Scientific Assessment of Stratospheric Ozone, Vol 11. World Meteorological Organization, Global Ozone Research and Monitoring Project Report No. 20, 1989
6. Wayne RP (2001) Chemistry of Atmospheres. Clarendon press, Oxford
7. Pinnock S, Hurly M, Shine KP, Wallington TJ, Smyth TJ (1995) J Geophys Res 100:23227–23238
8. International Panel on Climate Change (IPCC) (1996) Climate change 1995: the science of climate change. Cambridge University Press, New York
9. Tsai WT (2005) J Hazard Mater 119:69–78
10. Sekiya A, Misaki S (2000) J Fluorine Chem 101:215–221
11. Bivens DB, Minor BH (1998) Int J Refrig 21:567–576
12. Ravishankara RA, Turnipseed AA, Jensen NR, Barone S, Mills M, Howark CJ, Solomon S (1994) Science 263:71–75
13. Granier C, Shine KP, Daniel JS, Hansen JE, Lal S, Stordal F (1999) Climate effects of ozone and halocarbon changes, in scientific Assessment of Ozone Depletion: 1998 Rep. 44, Global Ozone Research and Monitoring Project. World Meteorological Organization, Geneva, Switzerland
14. Cooper DL, Cunningham TP, Allan NL, McCulloch A (1992) Atmos Env 26A:1331–1334
15. Cooper DL, Cunningham TP, Allan NL, McCulloch A (1993) Atmos Env 27A:117–119
16. Chen L, Kutsuna S, Tokuhashi K, Sekiya A (2006) J Phys Chem A 110:12845–12851
17. Urata S, Takada A, Uchimaru T, Chandra AK (2003) Chem Phys Lett 368:215–223
18. Chen L, Kutsuna S, Tokuhashi K, Sekiya A, Takeuchi K, Ibusuki T (2003) Int J Chem Kinet 35:239–245
19. Sun H, Gong H, Pan X, Hao L, Sun CC, Wang R, Huang X (2009) J Phys Chem A 113:5951–5957

20. Wallington TJ, Schneider WF, Sehested J, Blide M, Platz J, Nielsen OJ, Christensen LK (1997) J Phys Chem A 101:8264–8274
21. Atkinson R (1990) Atmos Environ 24A:1–41
22. Wallington TJ, Hurley MD, Fracheboud JM, Orlando JJ, Tyndall GS, Sehested J, Mogelberg TE, Nielsen OJ (1996) J Phys Chem 100:18116–18122
23. Christensen LK, Wallington TJ, Guschin A, Hurly MD (1999) J Phys Chem A 102:1854–1864
24. Good DA, Mike K, Randy S, Francisco JS (1999) J Phys Chem 103:9230–9240
25. Good DA, Francisco JS (1998) J Phys Chem A 102:1854–1864
26. Frisch MJ, Trucks GW, Schlegel HB et al. (2003) Gaussian 03, Rev C.02. Gaussian Inc, Pittsburgh, PA
27. Becke AD (1993) J Chem Phys 98:5648–5652
28. Lee C, Yang W, Parr RG (1988) Phys Rev B 37:785–789
29. Gonzalez C, Schlegel HB (1990) J Chem Phys 94:5523–5527
30. Curtiss LA, Raghavachari K, Trucks GW, Pople JA (1991) J Chem Phys 94:7221–7230
31. Curtiss LA, Redfern PC, Smith BJ, Radom L (1996) J Chem Phys 104:5148–5164
32. Mebel AM, Morokuma K, Lin MC (1995) J Chem Phys 103:7414–7421
33. Frisch A, Nielsen AB, Holder AJ (2000) GaussView Reference. Gaussian Inc, Wallingford, CT
34. Scott AP, Radom L (1996) J Phys Chem 100:16502–16513
35. Truhlar DG, Garrett BC, Klippenstein SJ (1996) J Phys Chem 100:12771–12800
36. Wigner EP (1932) Z Phys Chem B 19:203–216